

Helical Channel Mesoporous Materials with Embedded Magnetic Iron Nanoparticles: Chiral Recognition and Implications in Asymmetric Olefin Epoxidation

Cristina I. Fernandes,^a Gavin B. G. Stenning,^b James D. Taylor,^b Carla D. Nunes,^{a,*} and Pedro D. Vaz^{a,b,*}

^a COB, Departamento de Química e Bioquímica, Faculdade de Ciências da Universidade de Lisboa, Campo Grande, Ed. C8, 1749-016 Lisboa, Portugal

Fax: (+351)-217-500-088; phone: (+351)-217-500-876; e-mail: cmnunes@ciencias.ulisboa.pt

^b ISIS Neutron & Muon Source, Rutherford Appleton Laboratory, Chilton, Didcot, Oxfordshire OX11 0QX, U.K.
E-mail: pedro.duarte-vaz@stfc.ac.uk

Received: May 4, 2015; Revised: August 17, 2015; Published online: October 14, 2015



Supporting information for this article is available on the WWW under <http://dx.doi.org/10.1002/adsc.201500441>.

Abstract: In this work a mesoporous nanocomposite material comprising helical chiral channels and with embedded magnetic iron oxide nanoparticles in its Si-based MCM-41 type framework was synthesized. Afterwards, a bipyridine derivative was grafted to the inner surface used as ligand to coordinate a molybdenum(II) precursor complex. The Mo loading was found to be 2.42 wt% Mo, corresponding to 0.26 mmol_{Mo} g⁻¹. The successful preparation of this helical mesoporous material was evidenced by an extensive characterization process using powder XRD, SEM/TEM analysis, FT-IR and Raman spectroscopies, TGA analysis and also by SQUID measurements. Selective adsorption of enantiopure D- and L-phenylalanine shows that the material has a preference for the D- over the L- enantiomer. This provides evidence that the channels are chiral (although the particles are not) and that it is useful for chiral recognition applications. It also sets the explanation to

the good results achieved in the selective epoxidation of olefins. The resulting material was tested as catalytic precursor in the epoxidation of *cis*-cyclooctene, styrene, *R*-(+)-limonene and *trans*-hex-2-en-1-ol, using *tert*-butyl hydroperoxide (tbhp) as oxygen source. The catalytic studies show that the synthesized material yields selectively the desired epoxides of the tested substrates with very good results, especially at higher temperatures and using toluene as solvent. The major achievement of the catalyst was an outstanding stereocontrol of the reaction products imposed by the confined space of the helical chiral channels. Therefore these materials offer an important contribution to asymmetric catalysis and to fields where chiral recognition is a relevant concept.

Keywords: asymmetric catalysis; diastereoselectivity; epoxidation; heterogeneous catalysis; mesoporous materials; molybdenum

Introduction

Fostering the development of catalysts that yield selective processes is the aim of much research worldwide in both academia and industry. Particularly, the quest for selective olefin epoxidation processes is very important as epoxides are relevant building blocks across many areas. This is even more relevant when stereoselectivity is a must and not an option, such as in the pharmaceutical industry.

Several options are available, metal-centred catalysts being one of the most used ways to conduct such transformations in both homogeneous and heterogeneous catalysis. One advantage of the latter is that

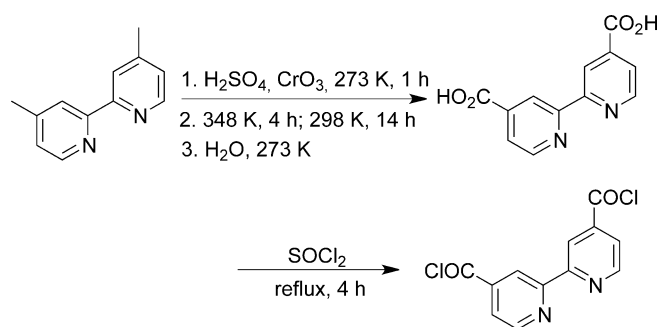
size and shape selectivity in porous inorganic catalysts is pivotal in a wide range of industrial and biological applications. In this respect enzymes are the model systems to pursue, therefore mimicking these biological factories in terms of exploring confined space environments was the driving force to prepare nanostructured mesoporous materials with helical morphology.^[1] This opened a new field of research due to their potential applications such as chiral selective separation, recognition and enantioselective catalysis.^[2–5] Such materials share with regular mesoporous materials (e.g., MCM-41, SBA-15, HMS) the same physical properties – wide pore openings and narrow pore size distribution – along with a high surface area

and the ability to prepare single-site active species across the high surface area for catalytic applications. In addition, these helical materials offer a tailored confined space which is capable of modulating reactions that are controlled by spatial constraints based on confined space as recently reported.^[6,7] At the end of the reactions the heterogeneous catalysts can be separated by filtration or centrifugation. More recently the advent of magnetic separation has triggered the development of magnetically separable catalysts which are easier to extract than using the processes mentioned earlier. Such catalysts have been developed with the aim of combining the properties of high surface area provided by porous materials with those from magnetic nanoparticles for an easy separation. Some examples rely on the introduction of the magnetic cores after the host porous material is prepared.^[8,9] Although efficient, this top-down approach may result in pore blockage and reduced catalytic activity. More recently, Thiel's group developed a bottom-up methodology to overcome such limitations.^[10] This was used to prepare mesoporous materials with previously prepared silica-coated magnetic nanoparticles embedded in the framework. The strategy proved to be adequate as the resulting catalyst proved to be active and stable.

Continuing our research on the development of stable, active and selective catalysts for olefin epoxidation,^[6,7] we describe in the present work the preparation of a magnetically separable mesoporous material with helical channels. To accomplish this we followed the bottom-up strategy adopted by Thiel and the resulting material was derivatized with a Mo complex anchored on the surface of the helical mesoporous silica with embedded magnetic iron oxide nanoparticles. This material was subsequently evaluated for its catalytic potential in olefin epoxidation reactions. As will be discussed throughout this work the strategy proved correct and the use of a material with helical channels led to enhanced stereoselectivity of products arising from the confined space shape of the channels.

Results and Discussion

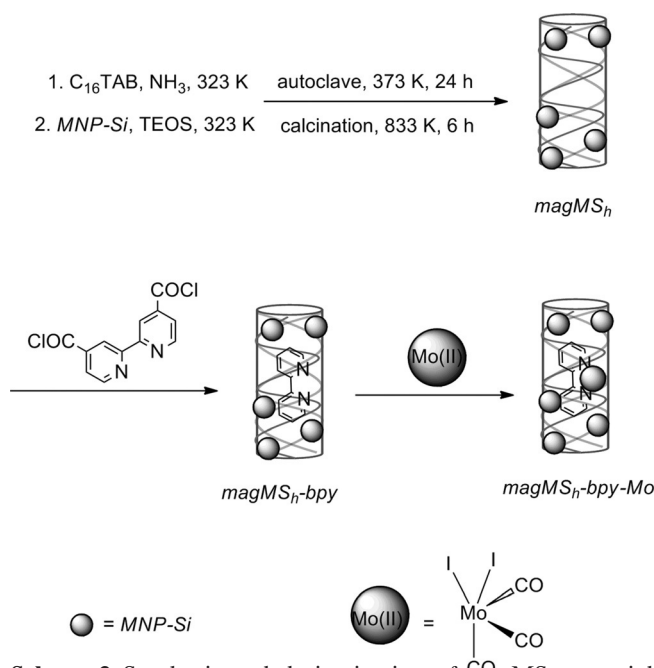
The helical mesoporous magnetic nanocomposite (*magMS_h*) was prepared using an entropy-driven procedure with achiral cationic surfactant template and ammonia in the presence of silica-coated magnetic nanoparticles (*MNP-Si*) that were co-condensed with tetraethoxysilane (TEOS), as described in the literature.^[10] In this particular case, we used cetyltrimethylammonium bromide (*C₁₆TAB*) and ammonia as surfactant and co-surfactant, respectively, according to a literature procedure.^[1]



Scheme 1. Synthesis of $(\text{ClCO})_2\text{-bpy}$ ligand for functionalization of *magMS_h* material.

Afterward, a bipyridine (*bpy*) derivative (Scheme 1) was used to coordinate the Mo(II) centre after being grafted to the inner silanol surface of the material.

Grafting of *bpy* ligand was straightforward by reacting $(\text{ClCO})_2\text{-bpy}$ with a suspension of *magMS_h* in acetonitrile. Afterward, the Mo(II) centre was introduced by suspending the *magMS_h-bpy* material in dichloromethane and then adding the $[\text{MoI}_2(\text{CO})_3(\text{CH}_3\text{CN})_2]$ precursor complex (Scheme 2). This afforded *magMS_h-bpy-Mo* material and according to elemental analysis, the Mo content was found to be 2.42 wt% Mo, corresponding to $0.26 \text{ mmol}_{\text{Mo}} \text{ g}^{-1}$. CHN elemental analysis of *magMS_h-bpy* revealed values of 5.91% C, 0.69% H, and 1.19% N. Given the N content, this result also shows that the loading of *bpy* derivative inside the pores is 0.43 mmol g^{-1} . This shows that the



Scheme 2. Synthesis and derivatization of *magMS_h* material with ligand *bpy* and Mo^{II} species.

Mo content is lower than the ligand loading reaching a ligand-to-metal ratio of 1.6 meaning that most probably all Mo complexes are coordinated to the *bpy* ligand.

All materials were characterized by DRIFT, powder XRD, SEM and TEM. Sorption/desorption N_2 isotherms were also carried out for textural parameters estimation. All spectroscopy and textural characterization features discussed in the following lines were found to be in agreement with related hybrid matrix mesoporous materials.^[1,6,10] The helical matrix of the as-prepared *magMS_h* material was confirmed by SEM and TEM measurements. SEM measurements (Figure 1a) show rod-shaped particles with helical morphology which are decorated with smaller round-shaped particles. The images provide evidence that the mesoporous silica rods have lengths ranging from 100s of nm to 2 μ m; the smaller round-shaped structures are the magnetic iron nanoparticles attached to the silica framework. TEM images show

rods with diameter ranging between 150 to 200 nm with helical morphology (Figure 1b); the images also illustrate the appearance of periodic lattice fringes (Figure 1b) along the rods, indicating the presence of helical channels within the rods, as reported before.^[1,6] The periodicity of the lattice fringes indicates that there was a regular environment of the channels where reactants and products may diffuse along without much disturbance. The TEM images also show darker spots which correspond to the magnetic nanoparticles. These nanostructures are embedded within the silica framework and evenly distributed across it. This makes clear that the synthetic procedure is adequate to prepare such mixed magnetic mesoporous materials with a homogeneous distribution of the nanoparticles throughout the framework (Figure 1b and c). Figure 1d also provides evidence that pore openings show a regular size distribution as evidenced by the pore size distribution curve discussed later in this work.

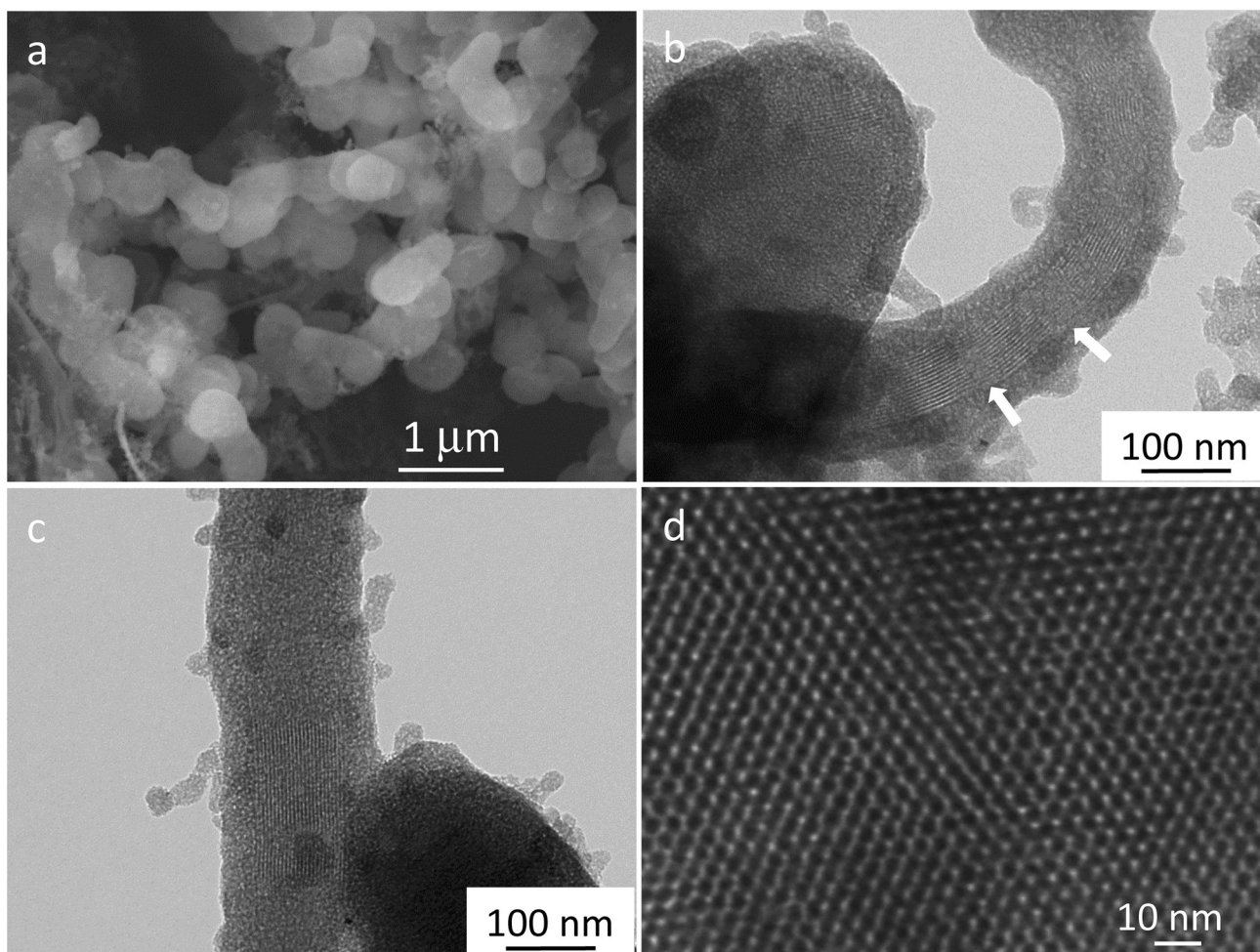


Figure 1. SEM image (a) of *magMS_h* material showing the morphology of the particles along with smaller size structures due to the magnetic iron oxide nanoparticles. TEM images are shown for the particles with helical channels (b) and magnified view perpendicular (c) and parallel (d) of the helical channels to the electron beam. Arrows in Figure b denote lattice fringes indicating the presence of helical channels with periodicity.

The local structure was also confirmed by powder X-ray diffraction measurements which agree with the published data and also make it possible to verify that the materials *magMS_h-bpy* and *magMS_h-bpy-Mo* are mesostructured.^[1,6] All resulting materials were of good quality according to the powder X-ray diffraction (XRD) patterns (Figure 2). The XRD patterns of the helical mesoporous magnetic material *magMS_h* exhibit four reflections indexed to a hexagonal cell as (100), (110), (200) and (210) in the 1.8–10° 2θ range (Figure 2a). In the 10–80° 2θ range a characteristic peak for the magnetite core (Fe₃O₄) was detected at around 35.5°, indexed to the (311) plane, revealing that magnetite nanoparticles are present as part of the porous silica framework and that their crystallinity was retained during the mesostructure formation (Figure 2b). This confirms observations made by SEM and TEM microscopy as discussed above. For material *magMS_h* the *d*₁₀₀ value for reflection (100) was estimated to be 4.03 nm, corresponding to a lattice constant of *a* = 4.66 nm (*a* = 2*d*₁₀₀/√3). Materials *magMS_h-bpy* and *magMS_h-bpy-Mo* obtained after subsequent stepwise functionalization with *bpy* and Mo(II), still show three reflections although with a slight deviation of the position maxima toward higher 2θ values as compared to *magMS_h*. For *magMS_h-bpy* material, the *d*₁₀₀ value is 3.95 nm, with a corresponding lattice constant of *a* = 4.56 nm; for *magMS_h-bpy-Mo* the values are, respectively, *d*₁₀₀ = 3.91 nm and *a* = 4.51 nm. The average crystallite size of the magnetic iron nanoparticles, estimated using the Debye–Scherrer equation, was found to be 22 nm, based on the peak indexed to the (311) plane at 2θ = 35.5°.

The powder XRD patterns of the *magMS_h* materials were found to provide similar results to those already reported by us for related systems.^[6,10–13]

The data from all materials are collected in Table 1, summarizing the relevant textural properties of the materials. The observed peak intensity reduction was common to all materials, being even more significant in the materials with the Mo core. This was not due to a crystallinity loss, but rather to a decrease in X-ray scattering contrast between the silica walls and the pore-filling material. This has been observed for other types of materials and was well documented in the literature.^[14,15]

Table 1. Textural parameters of host and composite materials, from powder XRD data and N₂ isotherms at 77 K, for all materials.

Material	2θ [°]	<i>d</i> ₁₀₀ [nm]	<i>a</i> [nm]	<i>S</i> _{BET} [m ² g ⁻¹] ^[a]	Δ <i>S</i> _{BET} [%]	<i>V</i> _P [cm ³ g ⁻¹]	Δ <i>V</i> _P [%] ^[b]	<i>d</i> _{BjH} [nm]
<i>magMS_h</i>	2.18	4.03	4.66	481	–	0.60	–	2.74
<i>magMS_h-bpy</i>	2.23	3.95	4.56	475	–1	0.56	–7	2.74
<i>magMS_h-bpy-Mo</i>	2.26	3.91	4.51	344	–28	0.46	–23	2.67

^[a] Surface area variation relative to parent *magMS_h*.

^[b] Total pore volume variation relative to parent *magMS_h*.

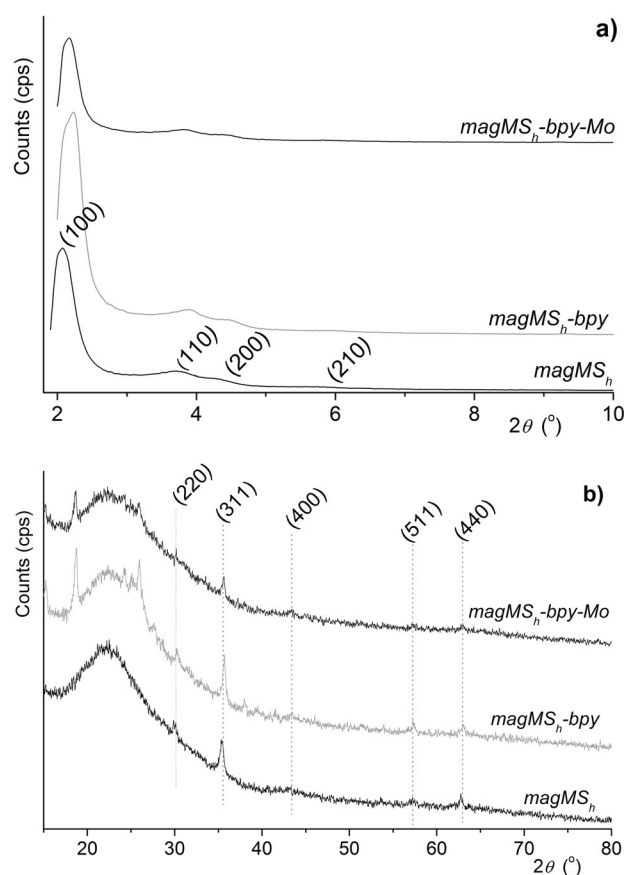


Figure 2. Powder XRD of *magMS_h*, *magMS_h-bpy* and *magMS_h-bpy-Mo* materials: (a) the small angle region (2° < 2θ < 10°) accounting for the mesoporous material; (b) the wide-angle region showing the peaks from the iron oxide magnetic nanoparticles. In both cases, most relevant peaks are shown with the corresponding indexation.

Nitrogen sorption/desorption studies at 77 K were also performed and have revealed that the *magMS_h* sample exhibits a reversible type IV isotherm (Figure 3a), typical of mesoporous solids (pore width between 2 nm and 50 nm, according to IUPAC).^[16] The calculated textural parameters (*S*_{BET} and *V*_P) of these materials (Table 1) agree with literature data.^[17,18] The capillary condensation/evaporation step in pristine *magMS_h* sample appears in the 0.30–0.45 relative pressure range, while the sharpness of this step re-

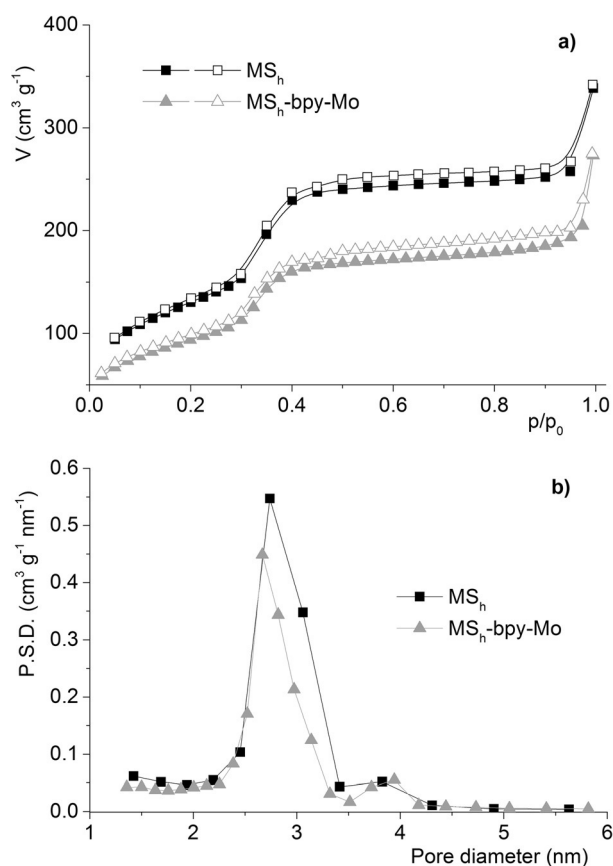


Figure 3. Nitrogen adsorption studies of $magMS_h$ and $magMS_h-bpy-Mo$ materials at 77 K: (a) isotherm; (b) pore size distribution curves. In the isotherm, both the adsorption (closed symbols) and desorption (open symbols) are shown.

flects a uniform size distribution. The functionalized material $magMS_h-bpy$ isotherm revealed a slightly lower N_2 uptake, accounting for the small decrease in both S_{BET} (−1%) and V_P (−7%). For the $magMS_h-bpy-Mo$ material, both S_{BET} and V_P parameters decrease more drastically by 28% and 23%, respectively. These results are in agreement with the p/p_0 coordinate decrease in the isotherm inflection points after post-synthesis treatments.^[19] Furthermore, the pore size distribution (PSD) curve maxima (Figure 3b), determined by the BJH method – d_{BJH} – for $magMS_h$ based materials change from 2.74 nm to 2.67 nm on going from $magMS_h$ to $magMS_h-bpy-Mo$ (Table 1).

Diffuse reflectance infrared spectroscopy (DRIFT) was used to characterize the hybrid materials, shown in Figure 4. The DRIFT spectrum of the $magMS_h$ material was typical of a silicate displaying a broad band in the 3600–2600 cm^{-1} range due to hydrogen-bonded silanol groups. Another important feature is the band at ca. 1630 cm^{-1} due to OH bending modes, while the intense broad band at 1239–950 cm^{-1} is assigned to the asymmetric stretching vibration modes of the mesoporous framework ($\nu Si-O-Si$).^[20] The immobilization of magnetic iron oxide nanoparticles coated

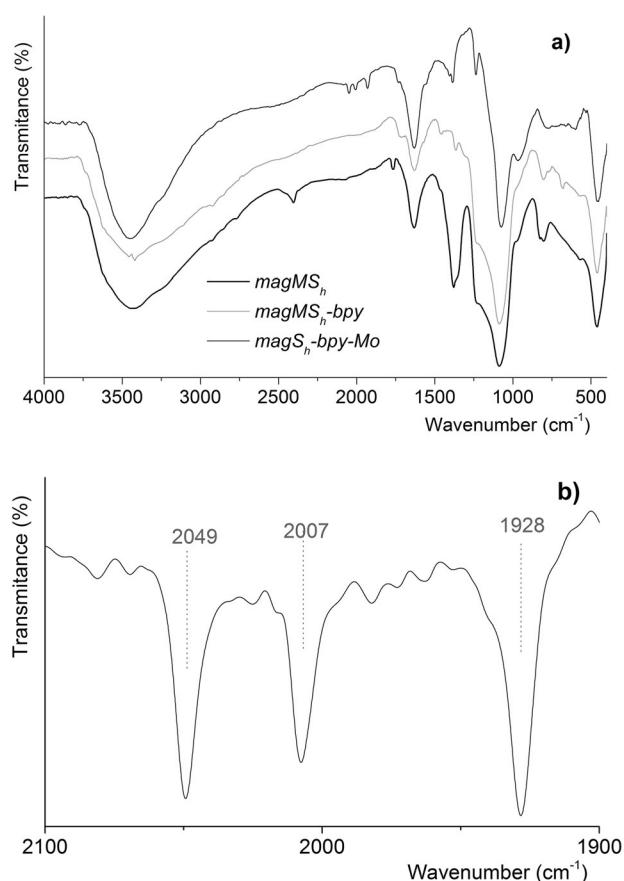


Figure 4. FT-IR spectra of $magMS_h$, $magMS_h-bpy$ and $magMS_h-bpy-Mo$ materials: (a) full mid-IR range; (b) zoomed image of the $\nu C=O$ modes region from $magMS_h-bpy-Mo$ material.

with silica ($MNP-Si$) on the surface of the mesoporous material was probed by the presence of characteristic bands of this type of nanoparticles, namely, an intense band at 451 cm^{-1} due to the $\nu Fe-O$ stretching mode and also a broad and intense band that appears at 1082 cm^{-1} due to the $\nu Si-O$ modes. After grafting of bpy ligand, affording material $magMS_h-bpy$, the DRIFT spectrum shows an overall similar profile dominated by the adsorptions of the host mesoporous material. Additionally, new bands were detected evidencing the ligand presence within the pores. The 1630 cm^{-1} band can be related with the $\nu C=N$ mode in addition to the OH bending mode of the matrix. Grafting of the bpy ligand was also monitored by probing its $\nu C=O$ mode. Neat $(ClCO)_2bpy$ ligand shows this mode at 1730 cm^{-1} , which agrees with the presence of the COCl group.^[21] After grafting, this mode is redshifted to 1714 cm^{-1} , which is compatible with the expected transformation resulting in the formation of silyl esters, as documented in the literature.^[6,22] In this way, the absence of the 1730 cm^{-1} band in the $magMS_h-bpy$ material strongly suggests that the bpy ligand is grafted to the inorganic matrix

in a bipodal fashion. After binding the molybdenum complex $[\text{MoI}_2(\text{CO})_3(\text{CH}_3\text{CN})_2]$, which affords material $\text{magMS}_h\text{-bpy-Mo}$, several changes/additional bands in the corresponding DRIFT spectrum are detected. The most striking feature is the observation of three bands at 2049, 2007 and 1928 cm^{-1} assigned to the $\nu\text{C}\equiv\text{O}$ modes (Figure 4b). These bands are shifted relatively to the $[\text{MoI}_2(\text{CO})_3(\text{CH}_3\text{CN})_2]$ precursor complex (observed at 2072, 2016 and 1921 cm^{-1}),^[7] being indicative of metal binding to the *bpy* ligand. Moreover, the fact that their shapes are symmetrical is indicative that the Mo cores are isolated enough, thus interacting through H-bonding. Additionally, the bands due to the $\nu\text{C}\equiv\text{N}$ vibrational modes from the acetonitrile (CH_3CN) ligands are not found, indicating that such ligands have been replaced by the immobilized ligand.

Figure 5 shows the thermogravimetric analyses (TGA) of the synthesized materials magMS_h , $\text{magMS}_h\text{-bpy}$ and $\text{magMS}_h\text{-bpy-Mo}$. All materials show some high temperature mass loss due to hydrox-

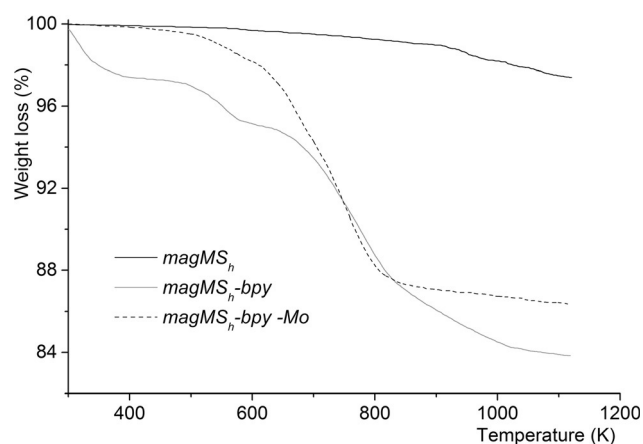


Figure 5. TGA profiles of magMS_h , $\text{magMS}_h\text{-bpy}$ and $\text{magMS}_h\text{-bpy-Mo}$ materials.

ylation of the mesoporous structure (clearly evidenced in magMS_h). Both $\text{magMS}_h\text{-bpy}$ and $\text{magMS}_h\text{-bpy-Mo}$ materials experience mass losses (less pro-

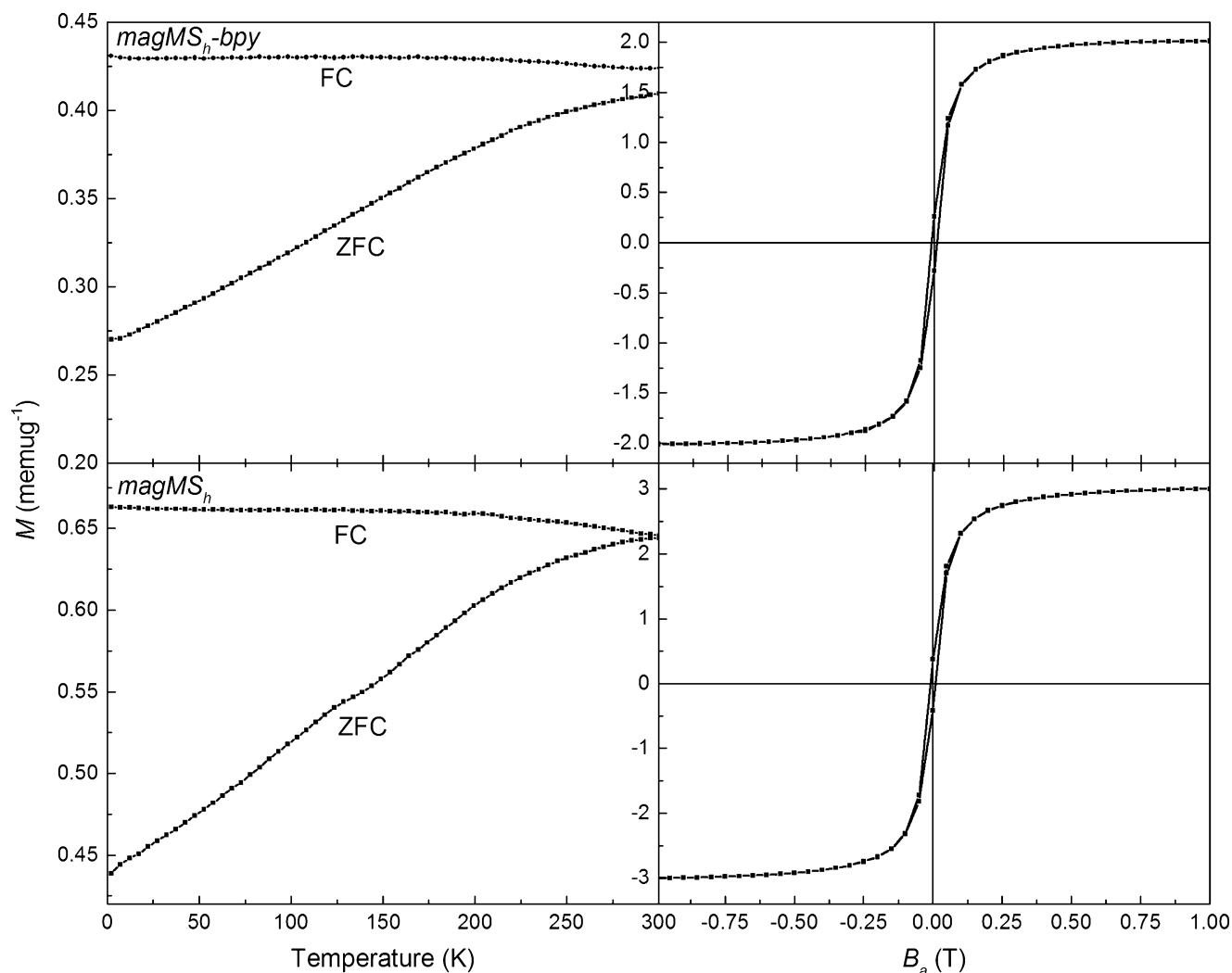


Figure 6. SQUID magnetometry of both $\text{magMS}_h\text{-bpy}$ and magMS_h .

nounced in the latter) corresponding to physisorbed water until 398 K. The $magMS_h$ -bpy derivative displays a 3-step degradation process occurring between 393 K and 833 K, with overall weight loss of 13.5%. Taking into account the high temperature mass loss observed in $magMS_h$ due to dehydroxylation, this leaves a net weight loss in $magMS_h$ -bpy material of 12% that can be assigned to loss of the ligand. This corresponds to 0.49 mmol g^{-1} of the ligand inside the mesoporous magnetic nanocomposite pores ($magMS_h$) being in agreement with the total amount of bpy (0.43 mmol g^{-1}) obtained from elemental analysis. Similar results were obtained for the $magMS_h$ -bpy-Mo material.

Figure 6 (top) shows the SQUID magnetometry for $magMS_h$ -bpy and $magMS_h$. The left hand side of the Figure is the temperature dependence of the samples both field-cooled (FC) and zero field-cooled (ZFC). The magnetic field was set to 100 Oe for temperature dependence and the data shown in Figure 6 were ac-

quired on warming the system. The right hand side of Figure 6 corresponds to the magnetic hysteresis loop. The hysteresis loops show similar saturation values, but a larger effect between $magMS_h$ -bpy and $magMS_h$ occurs between the splitting of FC and ZFC measurements of each.

Figure 7 shows again magnetometry of $magMS_h$ -bpy-Mo and $magMS_h$ -bpy-Mo (2) where the latter refers to an oxidized version after being exposed to catalytic conditions. Figure 6 and Figure 7 both show soft magnetic behaviour from the hysteresis loops with little or no magnetic anisotropy. With differing anisotropies this could have a very profound effect on this type of measurement.^[23] It can be noted that the saturation value and ZFC/FC measurements for $magMS_h$ -bpy-Mo give an increased value for when it has been oxidized, but is still smaller than those displayed in Figure 6. These results are consistent with those reported in the literature for a regular mesoporous magnetic nanocomposite.^[10]

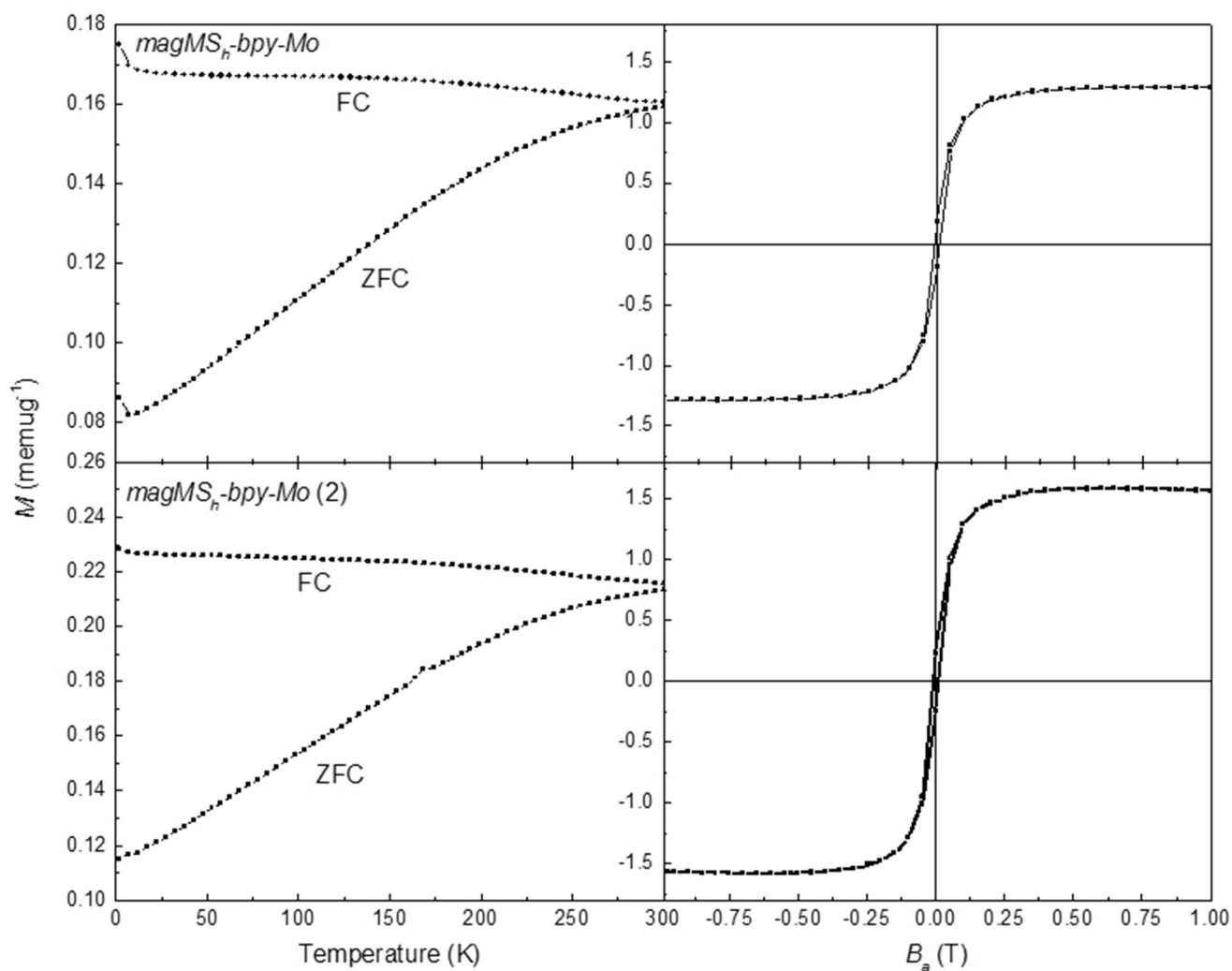


Figure 7. SQUID magnetometry of $magMS_h$ -bpy-Mo and $magMS_h$ -bpy-Mo (2).

The derivatized mesoporous magnetic nanocomposite material (*magMS_n-bpy-Mo*) was tested as a catalyst precursor for the epoxidation of two sets of substrates. The first one comprises simple olefins, such as *cis*-cyclooctene and styrene, while the second one includes multifunctional olefins, namely, *trans*-hex-2-en-1-ol and *R*-(+)-limonene. All reactions were carried out using *tert*-butyl hydroperoxide (tbhp) as oxygen donor, in different solvents, namely, acetonitrile, toluene and decane, at 353 K, 383 K and 393 K.

Special focus was dedicated to the stereoselectivity of products due to the specific helical features of the matrix, as already explored in a previous work.^[6] In this way, we analyzed the presence of the enantiomers/diastereomers in the products resulting from cat-

alysis with *trans*-hex-2-en-1-ol and *R*-(+)-limonene as substrates using a chiral GC column.

In the case of *cis*-cyclooctene, *magMS_n-bpy-Mo* material catalyzed selectively the oxidation of the substrate to the corresponding epoxide, without formation of any by-products (Table 2, entries 1–4). All *cis*-cyclooctene epoxidation reactions gave high yields of the corresponding epoxide (Figure 8a), namely, between 72 and 100%; however, the maximum yield (100%) was obtained at 383 K using toluene as solvent (Table 2, entry 3).

Styrene conversion is very efficient for all the tested temperatures and independent of the solvent. Despite this, selectivity for the epoxide is low, meaning that the major product is benzaldehyde. This

Table 2. Catalytic olefin epoxidation using *magMS_n-bpy-Mo* as catalyst.

Entry	Reaction ^[a]	Solvent	Temperature [K]	Conversion ^[b] [%]	Selectivity ^[b,c] [%]	<i>de</i> [%] ^[d]
1		acetonitrile	353	91	100	–
2		toluene	353	80	100	–
3			383	100	100	–
4		decane	393	72	100	–
5		acetonitrile	353	97	6 ^[e]	–
6		toluene	353	100	14 ^[e]	–
7			383	81	31 ^[e]	–
8		decane	393	87	22 ^[e]	–
9		acetonitrile	353	32	100	70 ^[f]
10		toluene	353	98	100	70 ^[f]
11			383	93	100	70 ^[f]
12		decane	393	79	100	74 ^[f]
13		acetonitrile	353	98	79 ^[g]	> 95 ^[h]
14		toluene	353	97 ^[i]	93 ^[g,j]	> 95 ^[h]
15			383	100 ^[i]	100 ^[i]	> 95 ^[h]
16		decane	393	98	83 ^[g]	> 95 ^[h]

^[a] All reactions were carried out in the presence of 200 mol% oxidant (tbhp) and 1 mol% Mo catalyst.

^[b] Calculated after 24 h, unless otherwise stated.

^[c] Calculated as “yield of epoxide”/“conversion” × 100%.

^[d] Determined by chiral GC.

^[e] Benzaldehyde formed as by-product.

^[f] Value refers to diastereomeric excess (*de*) of the *E* form.

^[g] α -Hydroxy ketone formed as by-product.

^[h] Although values of “100%” were measured, due to experimental error affecting measurements “> 95%” is reported instead.

^[i] After 6 h of reaction.

^[j] After 2 h of reaction.

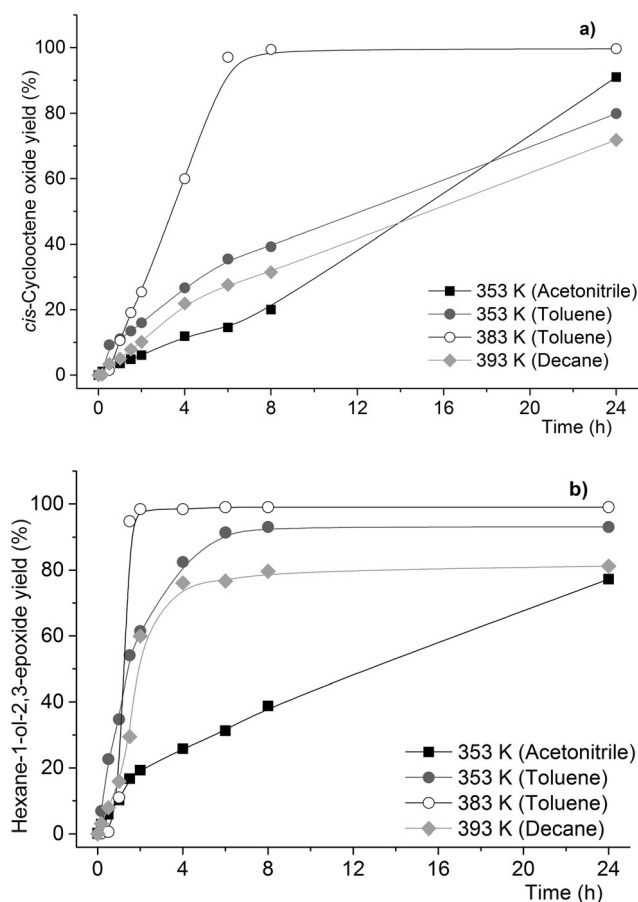


Figure 8. Kinetics of epoxidation of (a) *cis*-cyclooctene and (b) *trans*-hex-2-en-1-ol using *magMS_h-bpy-Mo* as catalyst obtained with different screening reaction.

product is formed through an oxidative cleavage mechanism from over-oxidation of styrene epoxide which further reacts to yield benzaldehyde. Formation of benzaldehyde in styrene oxidation experiments has already been reported in the literature for catalysts featuring magnetic separation capability.^[24–26]

R-(+)-Limonene is a substrate with two unsaturated C=C bonds, meaning that two different epoxides, the *endo*- and *exo*-cyclic isomers, are possible. In the present tests, the former was the favoured epoxide by the catalyst for all tests (Table 2, entries 9–12). It was possible to observe that in all reactions limonene epoxide was the sole product of *R*-(+)-limonene oxidation with good results (above 32%), as evidenced in Table 2 (entries 9–12).

These results were accompanied by very high substrate conversion, between 93% and 98%, when the solvent used was toluene (Table 2, entries 10 and 11). Even when the solvent is acetonitrile epoxide yields are very high, despite conversions being modest (Table 2, entry 9).

It was also possible to convert *trans*-hex-2-en-1-ol into its epoxide in all the tests made with very high

conversions. For example, almost 100% of conversion after only 2 h of reaction using toluene as solvent at 353 K and 383 K (Table 2, entries 14 and 15). The selectivity was also higher for all the tested temperatures. However, once again the use of toluene as solvent revealed to be the best method since it was possible to obtain a very high selectivity for the epoxide (above 95%) only after 2 h of reaction (Table 2, entries 14 and 15). Kinetic profiling of *trans*-hex-2-en-1-ol epoxidation shows that the catalysts present faster and higher conversion profiles when the solvent of reaction was toluene, for both temperatures, 353 K and 383 K (Figure 8b).

For example, in *R*-(+)-limonene epoxidation we observed that the catalyst follows the same trend, being sensitive to solvent and temperature. The reactions made with toluene gave higher conversion and selectivity for both temperatures (353 K and 383 K) as shown in Figure 9.

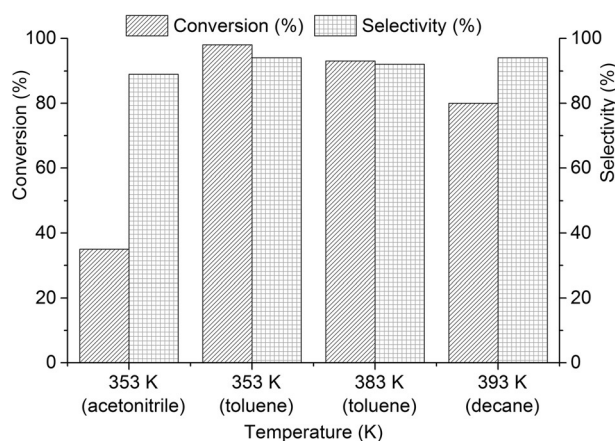


Figure 9. Conversion for *R*-(+)-limonene and selectivity for the corresponding endocyclic epoxide in the presence of *magMS_h-bpy-Mo* material across different reaction conditions.

Recyclability of the catalyst was evaluated across all experiments (see Table 3). In the case of *cis*-cyclooctene epoxidation the catalyst suffers severe deactivation, with conversion decreasing from 100% to 25% over 3 recycling experiments. The same trend was observed in *R*-(+)-limonene and *trans*-hex-2-en-1-ol epoxidations as well.

The exception to deactivation seems to be styrene oxidation, whose conversion levels were not affected to a great extent across recycling cycles and with little influence on the reaction kinetics.

To complete our studies we decided to evaluate the stereoselectivity of the *magMS_h-bpy-Mo* catalyst in the catalysis with *R*-(+)-limonene and *trans*-hex-2-en-1-ol due to the induced chirality of the magnetic mesoporous material, whose results are shown in Table 3. In the *R*-(+)-limonene epoxidation the stereoselectiv-

Table 3. Recyclability tests for the catalytic olefin epoxidation reactions using *magMS_n-bpy-Mo* as catalyst.

Entry	Reaction ^[a]	Solvent	Temperature [K]	Conversion ^[b,c] [%]	Selectivity ^[b,c,d] [%]
1		acetonitrile	353	91/77/62	100/100/100
2		toluene	353	80/57/31	100/100/100
3			383	100/30/25	100/100/100
4		decane	393	72/39/23	100/100/100
5					
6		acetonitrile	353	97/94/94	6/30/49 ^[e]
7		toluene	353	100/100/100	14/21/25 ^[e]
8		decane	393	87/100/98	31/32/33 ^[e]
9					
10		acetonitrile	353	32/19/9	100/100/100
11		toluene	353	98/85/39	100/100/100
12		decane	393	79/44/27	100/100/100
13					
14		acetonitrile	353	98/78/96	79 ^[f] /87 ^[f] /78 ^[f]
15		toluene	353	97 ^[g] /98/97	93 ^[f,g] /93 ^[f] /100
16		decane	393	100 ^[h] /97/97	100 ^[h] /86 ^[f] /89 ^[f]
17					
18					
19					
20					
21					
22					
23					
24					
25					
26					
27					
28					
29					
30					

^[a] All reactions were carried out in the presence of 200 mol% oxidant (tbhp) and 1 mol% Mo catalyst.

^[b] Calculated after 24 h, unless otherwise stated.

^[c] Multiple values correspond to recycling runs (1st–3rd).

^[d] Calculated as “yield of epoxide”/“conversion” × 100%.

^[e] In all experiments benzaldehyde formed as by-product.

^[f] Where “selectivity” < 100%, α -hydroxy ketone formed as by-product.

^[g] After 6 h of reaction.

^[h] After 2 h of reaction.

ity is high (between 70% and 74% of *de*). The best result was with decane as solvent at 393 K (Table 3, entries 9–12). Epoxidation of *trans*-hex-2-en-1-ol follows the same trend. In this case, epoxidation of the substrate was achieved with stereoselectivity above 95% (accounting for experimental errors, although in all cases “100%” was measured) across all tested conditions (temperature and solvent), as reported in Table 3 (entries 13–16). These results are in line with our previous work.^[6] It also means that the matrix backbone doping with magnetic iron oxide nanoparticles did not influence the quality of the helical channels as compared to the original non-magnetic *MS_n* material.^[1,6] Despite this, these results confirm that stereoselectivity was due to the rigid confined environment leading to substrate hindrance on approaching the catalytic active centre in the confined space of

the mesoporous helical host material. As discussed in our previous report,^[6] this arises from the described channel left-handedness, as stated in the original literature report^[1] (Fig. 3 in ref.^[1]) and the fact that the grafted *bpy* ligand may lie at saddle-shaped sites in the walls of the host material. This gives rise to a non-planar position of both *N*-donor atoms chelating Mo, yielding a confined environment imposed by the rigid inorganic matrix, which leads to enhanced stereocontrol over the catalytic reaction products.

In the catalytic experiments stereocontrol was achieved using the heterogeneous catalysts. Stereocontrol arose from the channel left-handedness similar to the related materials described in the literature (*cf.* Fig. 3 in ref.^[1]). This yields a confined environment imposed by the rigid inorganic matrix, leading to enhanced stereocontrol over the catalytic reaction products. Ac-

according to the authors who reported the original synthesis of MS_h materials,^[1] based on TEM observations, such helical materials have left-handed channels. Despite this, further evidence at the molecular level is required to make a proof of concept on chiral recognition for the *magMS_h* materials reported here, and to provide evidence that the chiral imprinting is not affected by introduction of the magnetic nanoparticles.

Chiral recognition was accomplished by adopting the literature procedure of Fernandes et al.^[6] To evaluate chirality of a given inorganic mesoporous material matrix we have adsorbed enantiopure D-phenylalanine and L-phenylalanine into the porous system of *magMS_h* materials.^[6] Results on the adsorption of enantiopure phenylalanine (D and L, with similar dimensions to the *cis*-cyclooctene, styrene and limonene substrates used) shows that *magMS_h* materials selectively adsorb much more D-phenylalanine (ca. 1.4-fold) after 24 h, as evidenced in Figure 10, showing a clear preference for D-phenylalanine over L-phenylalanine. This was found to be reproducible over 5 batches (each one run in triplicate) and strongly supports that the matrix channels are chiral. These results agree with previously reported results where similar discernment of enantiomers was accomplished by similar amounts.^[6,27] This experiment confirms that the observed left-handedness chirality of the channels was preserved, compared to the original materials without the magnetic capability,^[1,6] explaining the catalytic performance and the chiral recognition achievements.

The small error bars show that the synthesis procedure of such materials was reproducible based on a simple entropy-driven mechanism as discussed in the literature by Han et al.^[1] Therefore it strongly suggests that the channels in the inorganic matrix of *magMS_h* materials are really chiral with a focus on one predominant form. This study also confirms pre-

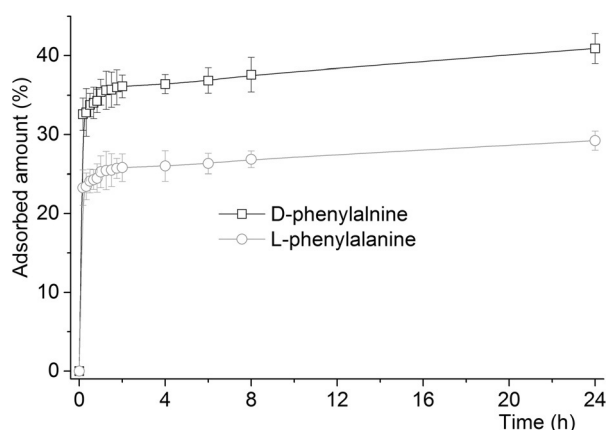


Figure 10. Adsorption kinetic profiles of pure L-phenylalanine and D-phenylalanine on *magMS_h* materials. The plot represents the average of 5 different synthesis batches each one tested in triplicate (error bars represent deviation from the average measured value).

vious observations made by Han et al. in the synthesis description of related materials where TEM data showed that MS_h materials are left-handed.^[1] Other authors have also addressed the issue of the nature of the chirality of the inorganic matrix in the literature.^[28]

This confined-space chiral concept imposed by the rigid inorganic backbone has been previously raised and discussed to explain similar stereoselectivity enhancements,^[29–35] where reactants are allowed to approach in a single orientation. Results in Table 2 support this concept by the observation of high stereoselectivity achieved for *trans*-hex-2-en-1-ol and *R*-(+)-limonene. In addition, data obtained from the selective adsorption of enantiopure amino acids support that MS_h materials can be used in processes where chiral recognition is valuable, such as catalysis or separation technology.

Conclusions

In this work we report the successful preparation of a mesoporous magnetic nanocomposite with embedded silica-coated iron oxide magnetic nanoparticles (22 nm average size) in a chiral mesoporous silica matrix by a one-pot direct synthesis methodology. This approach was based on the use of an entropy-driven procedure with an achiral cationic surfactant template. Then after the functionalization of the inner surface with a bipyridine-based ligand a subsequent coordination to a $[MoI_2(CO)_3]$ fragment was accomplished. The mesoscopic order and the helical pitch of the final materials depend on the use of ammonia. Additionally, the solid materials were, qualitatively and quantitatively, characterized by means of different spectroscopic techniques, which allowed a full depiction of the modified silica surface, corroborating the incorporation of the ligand into the inorganic helical rod mesoporous channels. The resulting material *magMS_h-bpy-Mo* was found to be an adequate catalyst for conducting olefin epoxidation reactions. We also noticed strong solvent effects affecting catalytic performance (mainly product selectivity). This issue is currently being assessed using neutron techniques.

The application of mesoporous materials with chiral helical channels conjugated with embedded magnetic nanoparticles in olefin epoxidation catalysis is reported for the first time. Compared to previous literature reports this material, holds all the properties of regular MS_h materials without embedded nanoparticles.^[1,6,36]

The performance in asymmetric catalysis was found to be outstanding across a range of olefins. In terms of enantioselective activity, the effect of the helical channel was found to have a positive influence on the diastereoselectivity of the epoxidation catalysis of dif-

ferent substrates. Other authors have reported similar achievements in other reactions with related materials.^[37] The observed stereoselectivity arises from the confinement effect imposed by the rigid inorganic chiral channels backbone. The introduction of the magnetic property allows an easy separation of the catalyst from reaction media and was found to be advantageous, as the catalysts are stable across several catalytic cycles and recycling easiness is welcome.

Experimental Section

Materials and Methods

All reagents except those that follow were obtained from Aldrich and used as received. Commercial grade solvents were dried and deoxygenated by distillation under nitrogen and kept over 4 Å molecular sieves (3 Å for acetonitrile). The complex $[\text{MoI}_2(\text{CO})_3(\text{CH}_3\text{CN})_2]$ was prepared according to the literature method.^[38] The silica coated iron oxide magnetic nanoparticles (MNP-Si) were also prepared according to a literature procedure.^[39]

FT-IR spectra were obtained as diffuse reflectance (DRIFT) measurements on a Nicolet 6700 in the 400–4000 cm^{-1} range using 2 cm^{-1} resolution.

Powder XRD measurements in the $2^\circ < 2\theta < 80^\circ$ range were taken on a Rigaku Miniflex 600 (theta/2theta) equipped with silicon strip detector and with automatic data acquisition, using a Cu source, using 40 kV and 15 mA. Samples were measured on glass slides.

Raman spectra were recorded on a Bruker Senterra dispersive microscope spectrometer equipped with cooled charge-coupled device (CCD) detector, using an excitation wavelength of 785 nm in the 100–4000 cm^{-1} range with 4 cm^{-1} resolution. The solid samples were put on top of glass slides and placed on the microscope plate for focusing the beam.

The N_2 sorption measurements were obtained on a Quantachrome Autosorb iQ porosimeter. BET specific surface areas (S_{BET} , P/P_0 from 0.03 to 0.30) and specific total pore volume V_p were estimated from N_2 adsorption isotherms measured at 77 K. The pore size distributions (PSD) were calculated by the Barrett–Joyner–Halenda (BJH) method from the desorption branch of the isotherm, using the modified Kelvin equation with correction for the statistical film thickness on the pore walls.^[40,41] The statistical film thickness was calculated using the Harkins–Jura equation in the p/p_0 range from 0.1 to 0.95.

Microanalyses for CHN and Mo quantitation were performed at CACTI, University of Vigo. CHN analyses were performed on a Fisons EA 1108; Mo quantification was performed on a Perkin–Elmer Optima 4300DV using In as internal standard.

SEM images were obtained on a Field Emission Gun Scanning Electron Microscope from JEOL, model JSM-7001F. TEM images were obtained on a Hitachi microscope, model H-8100 with a LaB_6 filament using an acceleration tension of 200 kV.

SQUID magnetometry measurements were performed on the Quantum design XL Magnetic Property Measurement

System (MPMS), capable of performing both AC and DC magnetometry both as a function of field and temperature. The magnetometer was able to measure in the temperature range from 400 K down to 1.8 K with applied magnetic fields of up to ± 7 T.

Synthesis of Ligand $(\text{CICO})_2\text{bpy}$

Synthesis of $(\text{CICO})_2\text{bpy}$ was by a two-step procedure found in the literature;^[21] the carboxylic acid was first prepared and then the acyl chloride was obtained through reaction with thionyl chloride.

Step 1: 4,4'-dimethyl-2,2'-bipyridine (Me_2bpy) (800 mg, 4.34 mmol) was dissolved in concentrated H_2SO_4 (10 mL) while cooling to 273 K. Once dissolved and cooled down, CrO_3 (2.6 g, 26.1 mmol) was very slowly added over a period of 1 h. The resulting greenish slurry and was then heated to 348 K for 4 h. After that time heating was turned off and the slurry was left stirring overnight at room temperature. The reaction was then quenched with ice/water. The green precipitate was separated by centrifugation and washed with deionized water (5×20 mL). The green powder was resuspended in deionized water and KOH was added under vigorous stirring until alkaline pH (~ 9) was reached. A blue residue was formed which was separated by centrifugation and washed with water (3×20 mL). The combined water extracts and the solution were acidified with concentrated HCl to pH ~ 1 making the carboxylic acid to be precipitated. The resulting white powder was centrifuged, washed with water, methanol and ether and then dried overnight in a vacuum oven at 313 K.

Step 2: SOCl_2 (5 mL, 25.7 mmol) [**ATTENTION: SOCl_2 is a reactive compound that can violently and/or explosively release dangerous gases upon contact with water and other reagents. It is toxic and will produce toxic gases; always handle in well vented fume hoods**] was added to the dry $(\text{HOOC})_2\text{bpy}$ (1 g, 4.1 mmol) and the mixture was refluxed for 3 h. The reaction was then evaporated to dryness yielding quantitatively the desired pure product. Overall yield was 82%. IR (KBr): $\nu = 3140$ ($\nu\text{C-H}$, s), 1727 ($\nu\text{C=O}$, vs), 1659 ($\nu\text{C=C}$, m), 1594 ($\nu\text{C=N}$, m), 658 cm^{-1} ($\nu\text{C-Cl}$, vs); $^1\text{H NMR}$ (400.13 MHz, CD_3OD , r.t.): $\delta = 9.14$ (s, H-6), 9.12 (d, H-3, $J_{\text{H-3,H-4}} = 6.8$ Hz), 8.43 (s, H-4); $^{13}\text{C NMR}$ (100.62 MHz, CD_3OD , r.t.): $\delta = 164.1$ (COCl), 148.3 (C-1), 147.5 (C-3), 144.6 (C-5), 126.6 (C-6), 123.3 (C-4).

Preparation of Heterogeneous Catalysts

Synthesis of material magMS_n : The helical mesoporous magnetic nanocomposite material (magMS_n) was prepared using an entropy-driven procedure with achiral cationic surfactant template. In this case, cetyltrimethylammonium bromide (C_{16}TAB) and ammonia as surfactant and co-surfactant, respectively, according to a literature procedure.^[6] In a typical material synthesis procedure, C_{16}TAB (1.0 g; 2.7 mmol) (Fluka, 96.0%) was dissolved in an aqueous ammonia solution (250 mL) (Sigma-aldrich, 25 wt%) at 323 K until complete dissolution. Then tetraethoxysilane (TEOS) (10 mL) (Aldrich, 98%) and MNP-Si (0.2 g) were added to the solution and the mixture was sonicated for about 5 min in order to disperse the nanoparticles. Following this, the solution was allowed to react for 3 h at 323 K under mechanical stirring in the presence of an inert N_2 atmosphere. After

this period, the mixture was transferred to a Teflon-lined stainless steel autoclave and aged at 373 K for 24 h. The product was separated by centrifugation, washed with water and ethanol several times and dried at 343 K in the oven. The surfactant occluded inside the pores of the material was then removed by calcination at 833 K for 6 h ($1^{\circ}\text{C min}^{-1}$).

Prior to the grafting experiments, physisorbed water was removed from the materials by heating at 453 K in vacuum (10^{-2} Pa) for 2 h. IR (KBr): $\nu=3413$ (vs), 1630 (s), 1379 (vs), 1209 (w), 1082 (vs), 964 (w), 796 (w), 451 cm^{-1} (s); powder XRD: $2\theta^{\circ}$ (*hkl* in parenthesis) = 2.18 (100), 3.87 (110), 4.36 (200), 5.99 (210), 35.50 (311).

Synthesis of material magMS_h-bpy: A suspension of the (ClCO)₂bpy ligand (0.281 g; 1 mmol) in acetonitrile (CH₃CN, 10 mL) was added to a magMS_h suspension (1 g) in acetonitrile (CH₃CN, 15 mL), and the mixture was stirred under a N₂ atmosphere at 358 K for 14 h. The resulting solid was filtered off and washed twice with dichloromethane (CH₂Cl₂, 2 × 10 mL) and then dried in vacuum at 323 K for 2 h. IR (KBr): ν : 3430 (vs), 3105 (w), 1766 (m), 1719 (m), 1630 (m), 1461 (w), 1384 (s), 1088 (vs), 976 (w), 833 (w), 686 (w), 465 cm^{-1} (s); powder XRD: $2\theta^{\circ}$ (*hkl* in parenthesis) = 2.26 (100), 3.91 (110), 4.51 (200), 5.92 (210), 35.70 (311); elemental analysis (%): found: C 5.91, H 0.69, N 1.19.

Synthesis of material magMS_h-bpy-Mo: A solution of [MoI₂(CO)₃(CH₃CN)₂] (0.300 g; 0.56 mmol) in dry dichloromethane (CH₂Cl₂, 10 mL) was added to a suspension of 1 g of magMS_h-bpy also in dry dichloromethane (CH₂Cl₂, 15 mL). The reaction mixture was stirred under a N₂ atmosphere at room temperature for 14 h. The resulting material was then filtered off, washed with dichloromethane (CH₂Cl₂, 2 × 10 mL), and dried under vacuum for 3 h. IR (KBr): $\nu=3429$ (vs), 3111 (w), 1712 (w), 1622 (m), 1458 (w), 1371 (w), 1088 (vs), 974 (w), 806 (w), 766 (w), 461 cm^{-1} (s); powder XRD: $2\theta^{\circ}$ (*hkl* in parenthesis) = 2.22 (100), 3.81 (110), 4.47 (200), 6.23 (210), 35.62 (311); elemental analysis (%): found: C 8.89, H 1.05, N 1.47, Mo 2.42.

General Procedure for Epoxidation Reactions

The materials were tested in epoxidation of olefins and allylic alcohols, such as *cis*-cyclooctene, styrene, *R*-(+)-limonene and *trans*-hex-2-en-1-ol, using *tert*-butyl hydroperoxide (tbhp) as oxidant (5.5 M in *n*-decane). The catalytic oxidation tests were carried out at different temperatures 353 K, 383 K and 393 K, using acetonitrile, toluene and decane as solvents, respectively. The reactions occurred under air in a reaction vessel equipped with a magnetic stirrer and a condenser. In a typical experiment, the vessel was loaded with olefin or alcohol (100 mol%), oxidant (200 mol%) and 3 mL of solvent. The final volume of the reaction was *ca.* 6 mL. The addition of the oxidant determined the initial time of the reaction. These reactions were conducted under a normal air atmosphere. Conversion, product yields and stereochemistry were monitored by sampling periodically and analyzing them using a Shimadzu QP2010-Plus GC/MS system and a capillary column (Teknokroma TRB-5MS/TRB-1MS or Restek Rt- β DEXsm) operating in the linear velocity mode. Recycling tests were carried out as described above using material magMS_h-bpy-Mo as catalyst; conversion and product yields were monitored as described above. After each cycle (24 h) the catalyst was filtered, washed

which CH₂Cl₂ several times and dried prior to reuse in a new catalytic cycle.

General Procedure for the Study of Channel Chirality in MS_h Materials

This study was based on a literature protocol by Fernandes et al.^[6] An aliquot of 50 mg of pure L-phenylalanine (or D-phenylalanine) was dissolved in 20 mL of MilliQ water followed by addition of 20 mg of template-free MS_h material previously activated. The mixture was magnetically stirred under ambient conditions and at a constant temperature of 298 K. The concentration of L-phenylalanine (or D-phenylalanine) was measured using UV spectroscopy (absorption at 260 nm) by sampling at regular time intervals. The procedure was applied to 5 different synthesis batches of MS_h materials and each one was tested in triplicate.

Acknowledgements

The authors thank FCT, POCI and FEDER (project UID/MULTI/00612/2013) for financial support. CIF also thanks FCT for a research grant (SFRH/BD/81029/2011).

References

- [1] Y. Han, L. Zhao, J. Y. Ying, *Adv. Mater.* **2007**, *19*, 2454–2459.
- [2] T. U. Gier, X. Bu, P. Feng, G. D. Stucky, *Nature* **1998**, *395*, 154–157.
- [3] D. Bradshaw, T. J. Prior, E. J. Cussen, J. B. Claridge, M. J. Rosseinsky, *J. Am. Chem. Soc.* **2004**, *126*, 6106–6114.
- [4] A. E. Rowan, R. J. M. Nolte, *Angew. Chem.* **1998**, *110*, 65–71; *Angew. Chem. Int. Ed.* **1998**, *37*, 63–68.
- [5] S. Che, Z. Liu, T. Ohsuna, K. Sakamoto, O. Terasaki, T. Tatsumi, *Nature* **2004**, *429*, 281–284.
- [6] C. I. Fernandes, M. S. Saraiva, T. G. Nunes, P. D. Vaz, C. D. Nunes, *J. Catal.* **2014**, *309*, 21–32.
- [7] R. A. García-Muñoz, V. Morales, M. Linares, B. Rico-Oller, *Langmuir* **2014**, *30*, 881–890.
- [8] M. Fröba, R. Köhn, G. Bouffaud, O. Richard, G. Tendeloo, *Chem. Mater.* **1999**, *11*, 2858–2865.
- [9] J. Lee, J. Kim, T. Hyeon, *Adv. Mater.* **2006**, *18*, 2073–2094.
- [10] S. Shylesh, L. Wang, S. Demeshko, W. R. Thiel, *ChemCatChem* **2010**, *2*, 1543–1547.
- [11] N. U. Silva, C. I. Fernandes, T. G. Nunes, M. S. Saraiva, C. D. Nunes, P. D. Vaz, *Appl. Catal. A: Gen.* **2011**, *408*, 105–116.
- [12] N. U. Silva, T. G. Nunes, M. S. Saraiva, M. Shalamzari, P. D. Vaz, O. C. Monteiro, C. D. Nunes, *Appl. Catal. B: Environ.* **2012**, *113*, 180–191.
- [13] A. C. Ventura, C. I. Fernandes, M. S. Saraiva, T. G. Nunes, P. D. Vaz, C. D. Nunes, *Curr. Inorg. Chem.* **2011**, *1*, 156–165.
- [14] B. Marler, U. Oberhagemann, S. Vortmann, H. Gies, *Microporous Mater.* **1996**, *6*, 375–383.

- [15] W. Hammond, E. Prouzet, S. D. Mahanti, T. J. Pinna-vaia, *Microporous Mesoporous Mater.* **1999**, *27*, 19–25.
- [16] J. Gregg, K. S. W. Sing, *Adsorption, Surface Area and Porosity*, Academic Press, London, 2nd edn., **1982**.
- [17] M. D. Alba, A. I. Becerro, J. Klinowski, *J. Chem. Soc. Faraday Trans.* **1996**, *92*, 849–854.
- [18] A. A. Romero, M. D. Alba, W. Zhou, J. Klinowski, *J. Phys. Chem. B* **1997**, *101*, 5294–5300.
- [19] M. Jaroniec, M. Kruk, J. P. Olivier, *Langmuir* **1999**, *15*, 5410–5413.
- [20] P. D. Vaz, C. D. Nunes, M. Vasconcellos-Dias, M. M. Nolasco, P. J. A. Ribeiro-Claro, M. J. Calhorda, *Chem. Eur. J.* **2007**, *13*, 7874–7882.
- [21] N. Garelli, P. Vierling, *J. Org. Chem.* **1992**, *57*, 3046–3051.
- [22] W. Bett, S. Cradock, *Monatsh. Chem.* **1980**, *111*, 193–198.
- [23] G. B. G. Stenning, G. J. Bowden, S. A. Gregory, P. A. J. de Groot, G. van der Laan, L. R. Shelford, P. Bencok, P. Steadman, A. N. Dobrynin, T. Hesjedal, *Phys. Rev. B* **2012**, *86*, 174420–1–174420–5.
- [24] C. I. Fernandes, N. U. Silva, P. D. Vaz, T. G. Nunes, C. D. Nunes, *Appl. Catal. A: Gen.* **2010**, *384*, 84–93.
- [25] W. Guo, G. Wang, Q. Wang, W. Dong, M. Yang, X. Huang, J. Yu, Z. Shi, *J. Mol. Catal. A: Chem.* **2013**, *378*, 344–349.
- [26] X. Huang, W. Guo, G. Wang, M. Yang, Q. Wang, X. Zhan, Y. Feng, Z. Shi, C. Li, *Mater. Chem. Phys.* **2012**, *135*, 985–990.
- [27] Z. Guo, Y. Du, Y. Chen, S.-C. Ng, Y. Yang, *J. Phys. Chem. C* **2010**, *114*, 14353–14361.
- [28] S. Yang, L. Zhao, C. Yu, X. Zhou, J. Tang, P. Yuan, D. Chen, D. Zhao, *J. Am. Chem. Soc.* **2006**, *128*, 10460–10466.
- [29] J. Wang, L. Zhao, H. Shi, J. He, *Angew. Chem.* **2011**, *123*, 9337–9342; *Angew. Chem. Int. Ed.* **2011**, *50*, 9171–9176.
- [30] M. D. Jones, R. Raja, J. M. Thomas, B. F. G. Johnson, D. W. Lewis, J. Rouzaud, K. D. M. Harris, *Angew. Chem.* **2003**, *115*, 4462–4467; *Angew. Chem. Int. Ed.* **2003**, *42*, 4326–4331.
- [31] R. Raja, J. M. Thomas, M. D. Jones, B. F. G. Johnson, D. E. W. Vaughan, *J. Am. Chem. Soc.* **2003**, *125*, 14982–14983.
- [32] M. R. Castillo, L. Fousse, J. M. Fraile, J. I. García, J. A. Mayoral, *Chem. Eur. J.* **2007**, *13*, 287–291.
- [33] R. A. García-Muñoz, V. Morales, T. Garcés, *J. Mater. Chem.* **2012**, *22*, 2607–2615.
- [34] R. A. García-Muñoz, R. van Grieken, J. Iglesias, V. Morales, N. Villajos, *J. Catal.* **2010**, *274*, 221–227.
- [35] T. Yamamoto, M. Suginome, *Angew. Chem.* **2009**, *121*, 547–550; *Angew. Chem. Int. Ed.* **2009**, *48*, 539–542.
- [36] L. Zhang, S. Q. Zhang, L. Cheng, Z. Yan, G. Q. M. Lu, *Nanotechnology* **2008**, *19*, 435608.
- [37] R. A. García-Muñoz, V. Morales, M. Linares, B. Rico-Oller, *Langmuir* **2014**, *30*, 881–890.
- [38] J. Gimenez, C. D. Nunes, P. D. Vaz, A. A. Valente, P. Ferreira, M. J. Calhorda, *J. Mol. Catal. A: Gen.* **2006**, *256*, 90–98.
- [39] C. I. Fernandes, M. D. Carvalho, L. P. Ferreira, C. D. Nunes, P. D. Vaz, *J. Organomet. Chem.* **2014**, *760*, 2–10.
- [40] M. Kruk, M. Jaroniec, *Langmuir* **1997**, *13*, 6267–6273.
- [41] M. Kruk, V. Antochshuk, M. Jaroniec, A. Sayari, *J. Phys. Chem. B* **1999**, *103*, 10670–10678.